The role of metals in catalysis by the restriction endonuclease *Bam*HI

Hector Viadiu[1] and Aneel K. Aggarwal[2]

Type II restriction enzymes are characterized by their remarkable specificity and simplicity. They require only divalent metals (such as Mg^{2+} or Mn^{2+}) as cofactors to catalyze the hydrolysis of DNA. However, most of the structural work on endonucleases has been performed in the absence of metals, leaving unanswered questions about their mechanisms of DNA cleavage. Here we report structures of the endonuclease *Bam*HI–DNA complex, determined in the presence of Mn^{2+} and Ca^{2+}, that describe the enzyme at different stages of catalysis. Overall, the results support a two-metal mechanism of DNA cleavage for *Bam*HI which is distinct from that of *Eco*RV.

Type II restriction endonucleases are phosphodiesterases that recognize short (four to eight base pairs) palindromic DNA sequences, and cleave both DNA strands to yield 5'-phosphate and 3'-hydroxyl groups as products[1,2]. Although they have been the workhorses of molecular biology for more than 20 years, their catalytic mechanisms have not been satisfactorily explained. The three dimensional structures of six type II endonucleases are presently known, including *Eco*RI[3], *Eco*RV[4], *Bam*HI[5–7], *Pvu*II[8,9], *Cfr*10I[10], and *Fok*I[11,12]. All except *Cfr*10I have been determined bound to their cognate DNA sites. The enzymes share little sequence homology but in all cases fold up to form a central β-sheet that is flanked by α-helices on both sides[2]. The active sites occur at one end of the central β-sheet and contain at least three superimposable residues that are critical for catalysis. Two of these residues are usually acidic — except in *Cfr*10I which has a serine — while the third residue is usually a lysine, except in *Bam*HI which has a glutamic acid. Divalent cations are essential for activity, with the fastest cleavage rates occurring with Mg^{2+}, although other ions (Mn^{2+}, Co^{2+}, Zn^{2+}, Cd^{2+}) are also functional. Calcium is an exception that shows an inhibitory effect on DNA cleavage[13].

Several models have been proposed to explain the catalytic mechanism of restriction endonucleases[14]. These models differ in the number of cations involved in catalysis and in the moiety that activates the attacking water molecule. For *Eco*RV a two metal mechanism was proposed based on the crystal structures determined in the presence of divalent cations and on studies examining the synergistic effects of calcium and manganese on catalysis[13,15]. An alternative substrate assisted mechanism with a single metal

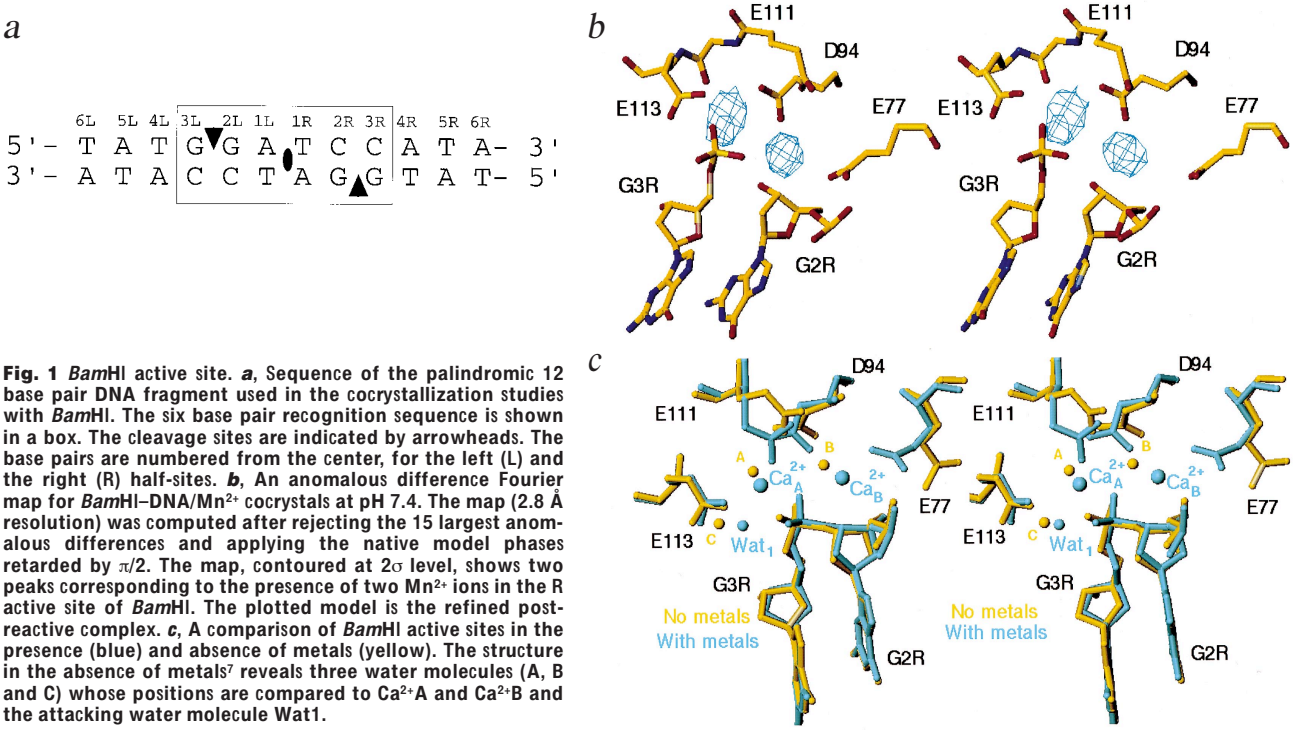

Fig. 1 ***Bam*HI active site. *a*, Sequence of the palindromic 12 base pair DNA fragment used in the cocrystallization studies with *Bam*HI. The six base pair recognition sequence is shown in a box. The cleavage sites are indicated by arrowheads. The base pairs are numbered from the center, for the left (L) and the right (R) half-sites. *b*, An anomalous difference Fourier map for *Bam*HI–DNA/Mn^{2+} cocrystals at pH 7.4. The map (2.8 Å resolution) was computed after rejecting the 15 largest anomalous differences and applying the native model phases retarded by π/2. The map, contoured at 2σ level, shows two peaks corresponding to the presence of two Mn^{2+} ions in the R active site of *Bam*HI. The plotted model is the refined post-reactive complex. *c*, A comparison of *Bam*HI active sites in the presence (blue) and absence of metals (yellow). The structure in the absence of metals[7] reveals three water molecules (A, B and C) whose positions are compared to Ca^{2+}A and Ca^{2+}B and the attacking water molecule Wat1.**

[1]Department of Biochemistry and Molecular Biophysics, Columbia University, New York, New York 10032, USA. [2]Structural Biology Program, Department of Physiology and Biophysics, Box 1677, Mount Sinai School of Medicine, 1425 Madison Avenue, New York, New York 10029, USA.

Correspondence should be addressed to A.K.A. *email: aggarwal@inka.mssm.edu*

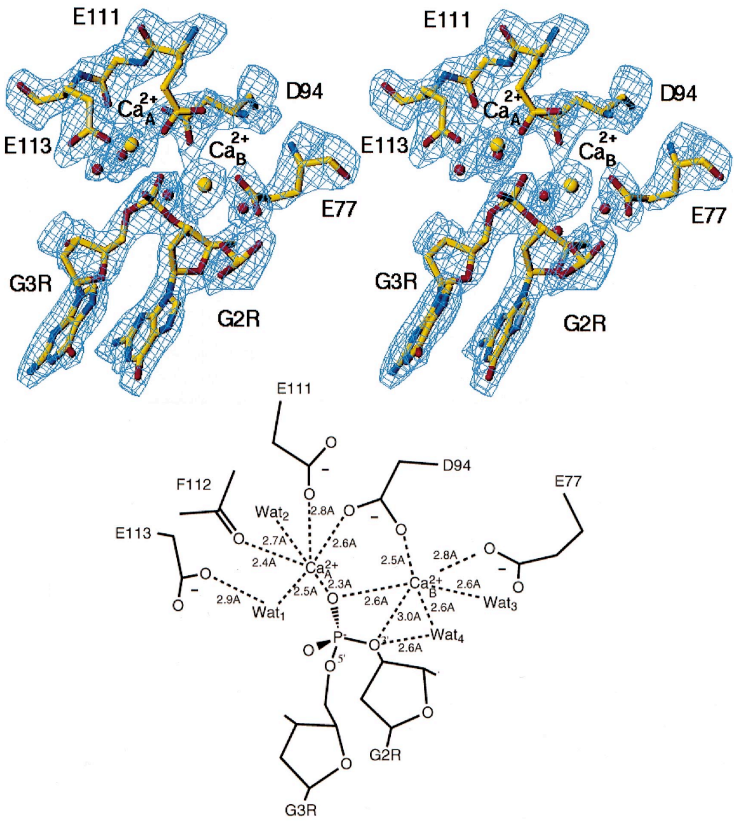

Fig. 2 A stereo view of the refined $2F_o - F_c$ map around the R active site of the calcium bound pre-reactive *Bam*HI–DNA complex. The active site residues (Glu 77, Asp 94, Glu 111 and Glu 113) and the DNA bases (Gua 2R and Gua 3R) adjoining the scissile phosphodiester have been labeled. The two calcium ions (Ca^{2+}A and Ca^{2+}B) are shown as yellow spheres. The water molecules are shown as small red spheres. A sketch summarizing the coordination geometries of Ca^{2+}A and Ca^{2+}B is shown at the bottom. Both ions are coordinated to six ligands in octahedral arrangements. Wat_1–Wat_4 refer to four water molecules within the active site

cation, has also been postulated for restriction enzymes, in which the phosphate group neighboring the scissile phosphodiester activates the attacking water molecule[16]. The debate over these different catalytic models has not been helped by the lack of structural information on metal binding. To date, *Eco*RV has been the only type II restriction endonuclease for which detailed metal bound structures were available[15,17].

The previous structures of *Bam*HI were determined in the absence of metals[5–7]. These structures revealed that the enzyme undergoes a series of conformational changes on DNA binding, the most striking of which is the unraveling of the C-terminal α-helices to form partially disordered arms. The arm of one monomer of *Bam*HI (the R subunit) fits into the DNA minor groove, while the arm of the other monomer (the L subunit) follows the DNA sugar-phosphate backbone. This introduces an asymmetry to the complex, but the active sites of both subunits (R and L) contain a similar clustering of acidic residues (Asp 94, Glu 111 and Glu 113) and water molecules around the scissile phosphodiesters[7].

Here we report crystallographic studies performed on *Bam*HI in the presence of Mn^{2+} and Ca^{2+}. We describe both the pre- and the post-reactive states of the enzyme. *Bam*HI maintains an active conformation as shown by the fact that the DNA can be cleaved directly in the crystals. Together, these results support a two-metal mechanism of catalysis for *Bam*HI that is distinct from *Eco*RV.

Results

First, we show using anomalous and isomorphous difference Fourier maps that the *Bam*HI active site contains two metal ions. Second, we provide a high resolution picture of the pre-reactive complex in which the inhibitory calcium ions are bound to the active site. Lastly, we describe the high resolution structure of the post-reactive complex, following the cleavage of the DNA in the crystal by the bound Mn^{2+} ions. We chose Mn^{2+} rather than Mg^{2+} because of its greater anomalous signal, making it easier to assign the ions unambiguously.

*Bam*HI active site contains two metals

We had previously hypothesized a two-metal mechanism of DNA cleavage for *Bam*HI based on the structure of the complex determined in the absence of metals[7]. The complex revealed three well defined water molecules in the active sites, two of which (A and B) were postulated to be replaceable by cations while the third was proposed to be the attacking water molecule[7]. To test this hypothesis we sought to determine the positions of the bound metals. The best evidence for a bound metal in an X-ray crystallography experiment is a peak in an anomalous difference Fourier map in which only the metal contributes significantly to the total anomalous signal[18]. Manganese has an anomalous signal of $2.8e^-$ at $\lambda = CuK\alpha$ that makes it ideal for such calculations. Thus, to locate the sites of divalent cations within the *Bam*HI active site, we measured data at $\lambda = CuK\alpha$ on a home rotating anode X-ray source, for cocrystals that were grown in the presence of $MnCl_2$ at pH 5.3, and for the same cocrystals after they had been soaked for an hour in $MnCl_2$ at pH 7.4. The anomalous difference Fourier maps calculated from these data revealed two peaks, A and B, that were 4.1 Å apart in the active site of the R subunit of *Bam*HI (Fig. 1*b*). Both peaks had a high signal to noise ratio (4.50 and 3.25σ in the $MnCl_2$ soaked map, for example) and were the most prominent peaks when the maps were displayed at a 2σ level. Site A is between Asp 94, Glu 111 and the scissile phosphate, while site B is next to the cleavable bond in a pocket formed by the side chains of Asp 94 and Glu 77 (Fig. 1*b*). Overall, the two sites are in similar positions to the two metals identified in the active site of the exonuclease domain of *E. coli* DNA polymerase I[19–21]. In comparison to the structure without metals[7], the cations are oriented similarly to waters A and B but are positioned deeper within the active site, enabling them to coordinate the active site residues Asp 94 and Glu 77. (Fig. 1*c*). In the structure without metals, residues Asp 94 and Glu 77 pointed away from the active site, probably to avoid the negatively charged DNA backbone[7]. However, upon metal binding both residues rearrange to face the DNA in order to coordinate the two metals.

Curiously, the two metal peaks occur only within the active site of the R subunit and not the L subunit of *Bam*HI. This is observed not only upon soaking the cocrystals with metals, but also in cocrystals grown in the presence of metals at low pH. It is possible that the kinetics of sequential cleavage at low pH are sufficiently slow to permit crystallization prior to the cleavage of both DNA strands. The R and L active sites differ markedly with a root-mean-square deviation (r.m.s.d.) of 1.4 Å between the active site residues (all atoms of residues Glu 77, Asp 94, Glu 111 and Glu 113). In particular, the L active site that lacks metals has a configuration similar to that of the structure without metals (r.m.s.d. of 0.7 Å) in which

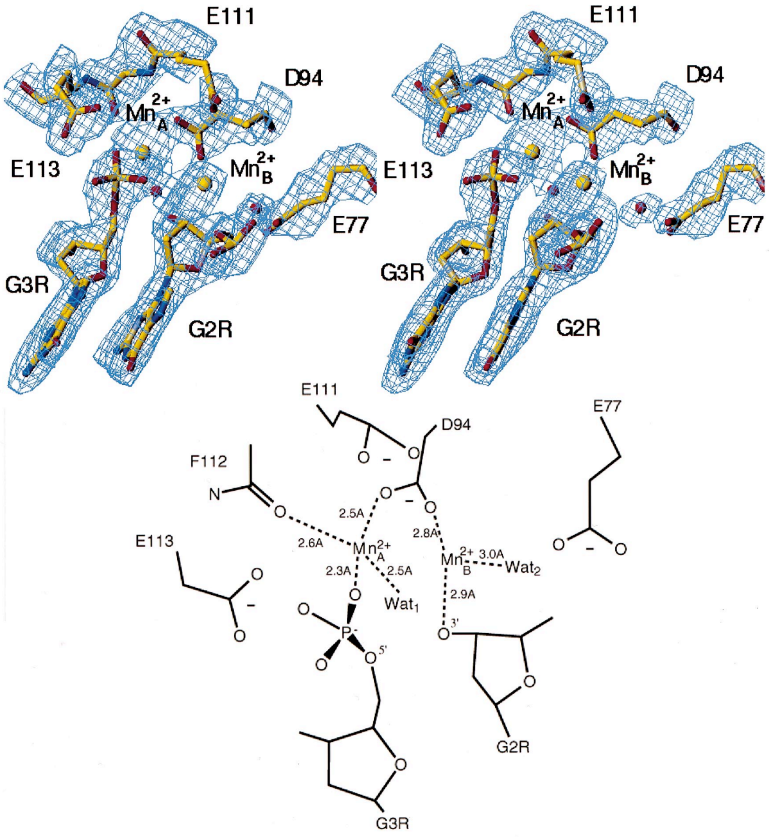

Fig. 3 A stereo view of the refined $2F_o$ - F_c map around the R active site of the manganese bound post-reactive *Bam*HI–DNA complex. Note that the scissile phosphodiester bond is cleaved in the cocrystal. The two manganese ions (Mn^{2+}A and Mn^{2+}B) are shown as yellow spheres. The water molecules are shown as small red spheres. A sketch summarizing the coordination geometries of Mn^{2+}A and Mn^{2+}B is shown at the bottom.

residues Asp 94 and Glu 77 point away from the DNA[7]. Asymmetric metal binding has also been observed with the *Eco*RV dimer. On soaking the *Eco*RV cocrystals with Mg^{2+}, Kostrewa and Winkler found that the metals were bound at only one of the active sites, accompanied by a shift in the DNA backbone towards the Mg^{2+} ions[15].

The pre-reactive complex

Calcium is an inhibitor of *Bam*HI as well as of other restriction enzymes such as *Eco*RV[13]. The mechanism by which Ca^{2+} inhibits DNA cleavage is unclear although kinetic studies with *Eco*RV have suggested that it competes with the binding of Mn^{2+} (or Mg^{2+})[13]. Thus to obtain a picture of the *Bam*HI–DNA pre-reactive complex prior to DNA cleavage, we sought to cocrystallize *Bam*HI with DNA in the presence of Ca^{2+} ions. The data for the Ca^{2+} complex were measured at the Cornell High Energy Synchrotron Source (CHESS) (λ = 0.908 Å). The $2F_o$ - F_c map revealed two broad peaks lying in between the carboxylic residues of the R active site and the DNA (Fig. 2). The positions of these peaks, presumably the Ca^{2+} ions, matched closely the positions of Mn^{2+} determined from the anomalous difference Fourier maps described above (Fig. 1*b*).

We have refined the Ca^{2+} complex to 2.0 Å resolution with an R-factor of 23.3% (Fig. 2). As expected, the phosphodiester bond stays intact in the presence of Ca^{2+}. The metals are separated by 4.3 Å and their coordination spheres are shown in Fig. 2. Ca^{2+}A is coordinated in an octahedral arrangement with six ligands: the Oδ2 of Asp 94 (2.6 Å), the Oε2 of Glu 111 (2.8 Å), the carbonyl oxygen of Phe 112 (2.4 Å), the O2 atom of the cleavable phosphate group (2.3 Å), and two water molecules (2.5 Å and 2.7 Å). Ca^{2+}B is also coordinated to six ligands: the Oδ1 of Asp 94 (2.5 Å), the Oε2 of Glu 77 (2.8 Å), the O2 and O3' atoms of the cleavable phosphate group (2.6 Å and 3.0 Å), and two water molecules (2.6 Å for both). Overall, the Ca^{2+} complex differs by only 0.54 Å r.m.s.d. in Cα positions from the complex determined in the absence of metals[7]. The main differences are in the R active site that binds calcium. The side chain of Asp 94 is coordinated in a bidentate manner to both Ca^{2+} ions, its conformation buttressed by hydrogen bonds to the hydroxyl group of Tyr 65 and the Oε1 of Glu 111. The movement of Glu 77 towards the active site is important in creating the binding site for Ca^{2+}B. (In the L active site that lacks calcium, Asp 94 and Glu 77 point away from the DNA in a similar manner as in the complex without metal[7]). Amongst the several water molecules at the R active site, two are noteworthy: Wat1, coordinated to Ca^{2+}A and 3.2 Å from the scissile phosphodiester group, is positioned ideally as the attacking water molecule, maintaining in-line orientation with the cleavable P-O3' bond (Fig. 2). The molecule is hydrogen bonded to Glu 113 (2.9 Å) which may act as a base in promoting its activation. The side chain of Glu 113 is fixed in position by a network of hydrogen bonds with the carbonyl oxygen of Ser 119, the Oγ atoms of Ser 119 and Ser 123, and the amine of residue 115. On the other side of the scissile phosphodiester group, Wat4, coordinated to Ca^{2+}B, forms a hydrogen bond (2.6 Å) with the O3', possibly acting as a general acid in donating a proton to the leaving group. Taken together, the Ca^{2+}-bound structure provides a remarkably detailed view of the *Bam*HI–DNA complex in its ground state, prior to DNA cleavage (Fig. 2).

The post-reactive complex

To visualize the *Bam*HI–DNA complex after the cleavage reaction, we refined the structure of a cocrystal that had been soaked for nine hours in a solution of $MnCl_2$. The data were again measured at CHESS (λ = 0.908 Å). Remarkably, the DNA is cleaved in the cocrystal — showing that *Bam*HI maintains an active conformation in the crystalline state (Fig. 3). (Interestingly, the cocrystal developed small fractures in the first few minutes of the soak, but these gradually disappeared to produce an intact crystal). The DNA cleavage occurs only in the R active site that contains two Mn^{2+} ions (Fig. 3). The overall r.m.s.d. between the Cα positions of the pre-reactive Ca^{2+} complex and the post-reactive Mn^{2+} complex is only 0.33 Å. The main difference is in the location of the scissile phosphate group after cleavage (Fig. 4*a*). Following cleavage, the phosphate group is displaced by 2.5 Å from the position it occupied when the phosphodiester bond was intact, bringing it within the vicinity of Glu 113 (3.0 Å) (Fig. 4*a*). The two Mn^{2+} ions are disposed similarly to the Ca^{2+} ions though they are slightly closer (3.9 Å as opposed to 4.3 Å). The coordination spheres of the two Mn^{2+} ions are, however, somewhat looser than Ca^{2+} (Fig. 3). Mn^{2+}A is coordinated by the Oδ2 of Asp 94 (2.5 Å), the carbonyl oxygen of Phe 112 (2.6 Å), the O2 atom of the cleaved phosphate group (2.3 Å) and a water molecule (2.5 Å). Glu 111 is no longer coordinated to the metal at site A as in the Ca^{2+} complex, but has

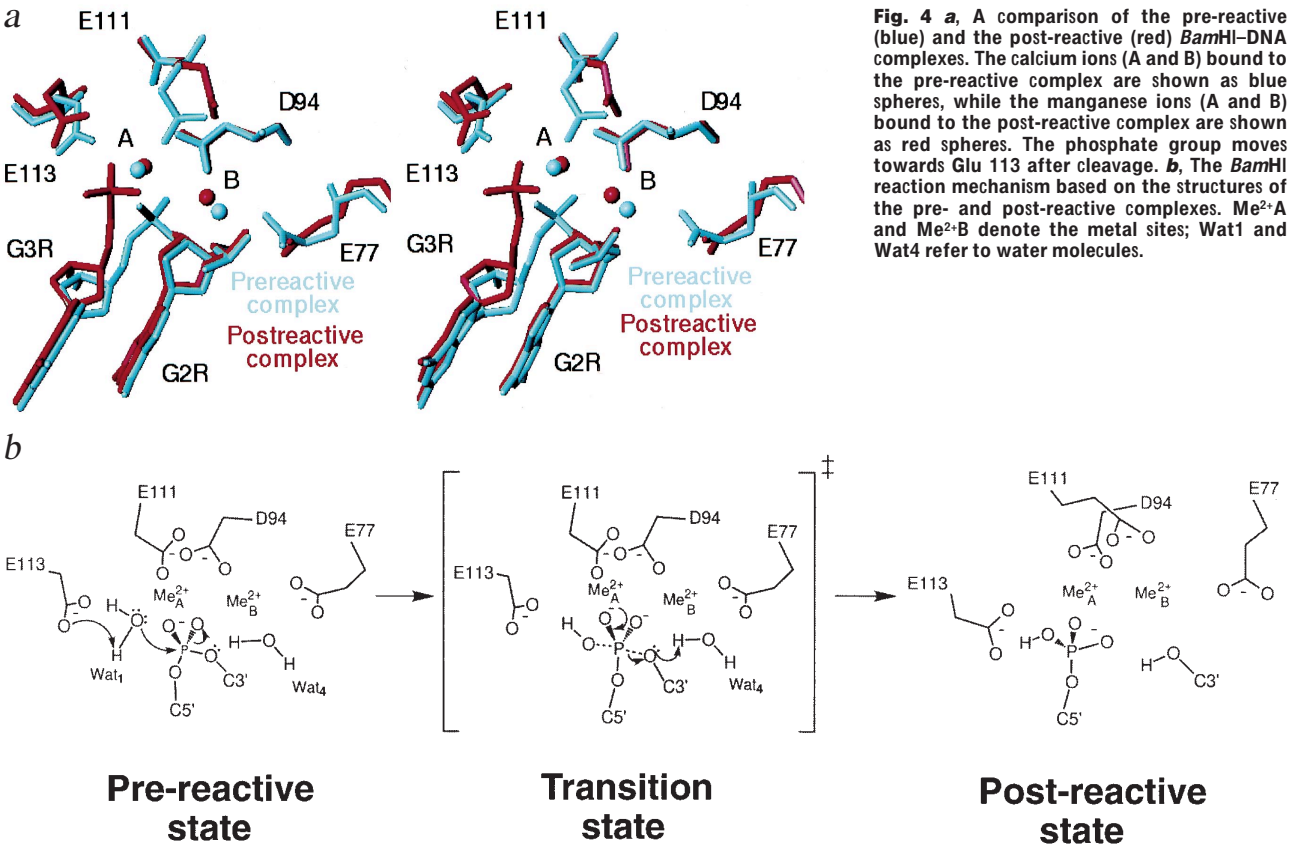

Fig. 4 ***a***, A comparison of the pre-reactive (blue) and the post-reactive (red) *Bam*HI–DNA complexes. The calcium ions (A and B) bound to the pre-reactive complex are shown as blue spheres, while the manganese ions (A and B) bound to the post-reactive complex are shown as red spheres. The phosphate group moves towards Glu 113 after cleavage. ***b***, The *Bam*HI reaction mechanism based on the structures of the pre- and post-reactive complexes. $Me^{2+}A$ and $Me^{2+}B$ denote the metal sites; Wat1 and Wat4 refer to water molecules.

moved nearer to the metal at site B. $Mn^{2+}B$ is coordinated by Oδ1 of Asp 94 (2.8 Å), the O3' of the Gua 2R (2.9 Å) and a water molecule (3.0 Å), but has lost its contacts with Glu 77 (Fig. 3). Overall, the metals give the impression of being less tightly bound after the cleavage reaction, which is also reflected by their higher temperature factors (45 $Å^2$ and 76 $Å^2$ for Mn^{2+} *versus* 31 $Å^2$ and 24 $Å^2$ for Ca^{2+} at sites A and B respectively).

Discussion

Type II restriction enzymes require only Mg^{2+} (or Mn^{2+}) as a cofactor to catalyze the hydrolysis of DNA phosphodiesters[1]. The reaction occurs through an S_N2 mechanism, with an in-line displacement of the 3'-hydroxyl group and an inversion of configuration of the 5'-phosphate group[22,23]. The important elements of the reaction are an activated water molecule to carry out the nucleophilic attack, a Lewis acid to stabilize the negatively charge transition state, and, in some cases, a general acid to donate a proton to the leaving O3' atom. The active sites of *Eco*RI, *Eco*RV, *Bam*HI, *Pvu*II, *Cfr*10I and *Fok*I are structurally similar, containing overlapping residues that occur at one end of a central β-sheet. The residues follow the weak consensus Glu/Asp-X_n-Glu/Asp/Ser-Z-Lys/Glu, where n varies from 9–18 residues and Z is usually a hydrophobic residue. The first two residues of the consensus, corresponding to Asp 94 and Glu 111 in *Bam*HI, are generally acidic, except for *Cfr*10I which has a serine[10]. The third residue is a lysine in all of the endonucleases except *Bam*HI, which has a glutamic acid (Glu 113). A fourth, acidic residue often precedes the consensus in some of the enzymes (Glu 77 in *Bam*HI), but it shows poor superposition[2].

We present evidence that *Bam*HI employs a two metal mechanism of DNA cleavage, similar to that proposed for the 3'-5'-exonuclease domain of the *E.coli* DNA polymerase I[20]. We show that the *Bam*HI active site contains two divalent cations (A and B) that are separated by ~4 Å and are coordinated by Glu 77, Asp 94 and Glu 111 (Fig. 1*b*). A detailed view of the *Bam*HI ground state is provided by the pre-reactive calcium complex, which we have refined to a high resolution of 2.0 Å. In addition to the two Ca^{2+} ions the structure reveals a candidate attacking water molecule (bound to $Ca^{2+}A$), and a water molecule that can donate a proton to the leaving group (bound to $Ca^{2+}B$) (Fig. 2). The picture that emerges from a consideration of all of the structures is as follows (Fig. 4*b*). Metal A activates the attacking water molecule, while metal B stabilizes the build-up of negative charge on the leaving O3' atom. At the same time, both metals (acting as Lewis acids) help to stabilize the pentacovalent transition state (Fig. 4*b*). A metal-bound water molecule has a lower pK_a value (11.4 and 10.6 for Mg^{2+} and Mn^{2+} respectively) than bulk water, favoring the formation of a nucleophilic hydroxyl species that can attack the scissile phosphodiester[24]. The positions of the Ca^{2+} and Mn^{2+} ions conform to the classical description of a two-metal mechanism, as discussed by Beese and Steitz for *E.coli* DNA polymerase I[20]. The two metals lie on a line that is parallel to the apical direction of the trigonal bipyramid geometry that would be expected at the scissile phosphodiester, during the transition state. The distance between the two metals (~4 Å) correlates with the anticipated distance of 3.8 Å between the apical oxygens in the transition state. Thus, the ions are in positions to stabilize the 'entering' and 'leaving' oxygens at the apical positions, and to reduce the energy in forming the 90° O–P–O bond angles between the apical and the equatorial oxygens.

A two-metal mechanism has also been postulated for *Eco*RV[13,15], but the crystallographically determined metal positions in that case are strikingly different from *Bam*HI (Fig. 5). In particular, the

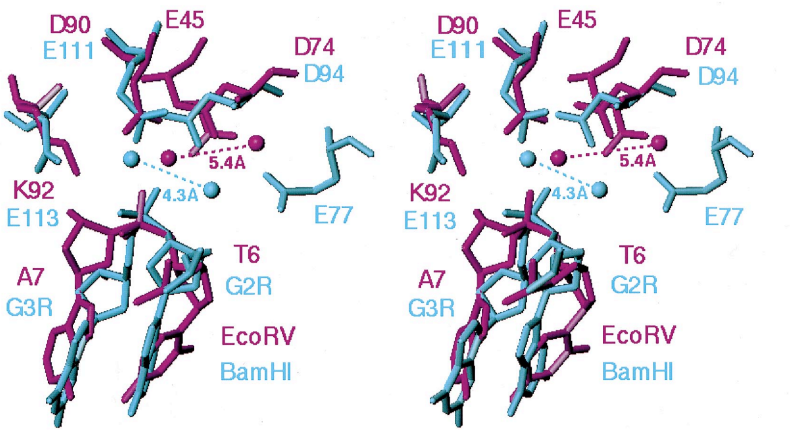

Fig. 5 A comparison of the *Bam*HI (blue) and the *Eco*RV (magenta) active sites, prior to DNA cleavage. The bound metals differ both in separation and in their relative positions in the two enzymes.

*Eco*RV metals (Mg^{2+} 1 and Mg^{2+} 2) are separated by ~5.4 Å and lie in the equatorial plane of the trigonal bipyramid[15] (Fig. 5). Mg^{2+} 1 is located approximately in between the metal sites A and B of *Bam*HI, while Mg^{2+} 2 is coordinated to Glu 45, a residue that has no counterpart in *Bam*HI. In the case of *Eco*RI only a single metal has been implicated for its catalysis based on structural and metal competition studies[13,25].

*Bam*HI is the only restriction endonuclease to be characterized structurally that has a glutamic acid (Glu 113) in the position corresponding to a lysine in the others. This difference is critical, as shown by the severe loss of cleavage activity when Glu 113 in *Bam*HI is substituted by a lysine residue[26], or conversely, when Lys 92 in *Eco*RV or Lys 113 in *Eco*RI is substituted by a glutamic acid residue[27,28]. Glu 113 lies in the vicinity of metal A and appears to act as a base in accepting a proton from the attacking water molecule. This correlates with studies showing that mutating Glu 113 to an aspartic acid has only a 10-fold effect on cleavage while changing it to glutamine or asparagine leads to a severe loss of cleavage activity (J. Bitinaite and I. Schildkraut, unpublished observation). Although Glu 113 is not directly coordinated to metal A its negative charge may also contribute to the binding of the metal.

The *Bam*HI scissile phosphate group occupies a different position before and after cleavage (Fig. 4*a*). We can carry out cleavage of the DNA in the crystals by soaking the cocrystals in $MnCl_2$. The cocrystals show small fractures in the first few minutes of the soak, which eventually 'heal' to produce an intact crystal. The experiment shows vividly that *Bam*HI maintains an active conformation in the crystal state. The fractures probably arise from changes in the positions of the DNA and protein atoms in forming the transition state. However, these atomic movements must be relatively small since they appear to be accommodated within the crystal lattice. By contrast, a similar soaking experiment with EcoRV did not support DNA cleavage, though it led to metal binding[15]. This could be explained if the EcoRV–DNA complex needs to undergo a more substantial distortion for catalysis[17]. Following cleavage by *Bam*HI, the phosphate group moves by 2.5 Å to within a hydrogen bonding distance of Glu 113 (Figs 3, 4*a*). One wonders whether the proton acquired by Glu 113 in its role as a base may be the basis for a hydrogen bond with the scissile phosphate group after cleavage. The two Mn^{2+} ions stay bound to the post-reactive complex, but have higher temperature factors than Ca^{2+}. This may indicate some weakening of the interactions with the metals, as a prelude to the dissociation of the enzyme from the cleaved product. Mn^{2+}+B in particular has a very high temperature factor (76 $Å^2$) suggesting that it may be only partially occupied after cleavage. The recently reported pre- and post-cleavage structures of intron-encoded endonuclease I-*Ppo*I also suggest a weakening of interactions between a metal and the leaving O3' leaving group after cleavage[29]. Besides the active site, there are few other changes at *Bam*HI–DNA interface following cleavage. The similarity of the *Bam*HI–DNA complex structures before and after cleavage is consistent with the comparable association rates measured for *Bam*HI for the intact (6.0×10^5 M^{-1} s^{-1}) and nicked (2.8×10^5 M^{-1} s^{-1}) DNA substrates[30].

*Bam*HI recognizes DNA in an asymmetric manner, in which the C-terminal arm of the R subunit goes into the DNA minor groove while the corresponding region of the L subunit follows the DNA sugar-phosphate backbone[7]. In all of our structures, the metals are only found in the R active site. This is true whether the cocrystals were obtained by soaking or growing them in the presence of metals. What could be preventing the binding of metals to the L-subunit? One possibility is that an interaction between Lys 205 of the asymmetric C-terminal arm of the L subunit and Glu 77, results in pulling Glu 77 away from the L active site. Glu 77 is one of the key residues that helps to coordinate metal ion B in the R active site, and its displacement in the L active site may therefore be one of the factors contributing to the asymmetry of metal binding in *Bam*HI. An intriguing question is whether this asymmetry in metal binding is related to the mechanism of the enzyme. *Bam*HI cleaves DNA in a sequential manner in which the enzyme cleaves first one DNA strand and then the other[30]. It appears that only the subunit with the C-terminal arm in the minor groove is able to bind metals for catalysis. When *Bam*HI binds DNA, it is possible to imagine a competition as to which subunit first manages to get its C-terminal arm into the minor groove. At a later time, as the two subunits exchange their C-terminal arms, the second subunit may then acquire the ability to bind metals for the cleavage of the second DNA strand.

Calcium provides an effective way of visualizing the enzyme before catalysis. Ca^{2+} is an effective inhibitor of restriction enzymes as well as nucleases such as *E. coli* DNA polymerase I and the *Tetrahymena* ribozyme[13,20,31]. The inhibitory effects of Ca^{2+} on restriction endonucleases have been ascribed to direct competition for the Mg^{2+} or Mn^{2+} binding sites, rather than any impact on the folding of the enzymes[13]. This is borne out in our structure, which reveals two Ca^{2+} ions bound at similar sites as the Mn^{2+} ions (Figs 2, 4*a*). The Ca^{2+} complex is well poised for catalysis with an attacking water molecule, and a water molecule that is in a position to protonate the leaving O3' atom. Despite this seemingly ideal geometry, the reaction does not proceed and the scissile P-O3' bond stays intact. To understand the mechanism of Ca^{2+} inhibition, we first note that the pK_a of a Ca^{2+} bound water ($pK_a = 12.9$) is higher than that for Mg^{2+} ($pK_a = 11.4$) or Mn^{2+} ($pK_a = 10.6$)[24]. This will have the effect of lowering the concentration of metal-hydroxyl ions for the nucleophilic attack on the scissile phosphodiester. Secondly, Ca^{2+} is a relatively bulky ion, with a radius of 0.99 Å as compared to 0.65 Å and 0.80 Å for Mg^{2+} and Mn^{2+} respectively[32]. Although, the two Ca^{2+} ions appear to be well accommodated in the ground state of the *Bam*HI–DNA complex, this may not be the case during the transition state. In particular, the crowding of oxygens in the equatorial plane of the trigonal bipyramid of the transition state may cause steric interference with the larger Ca^{2+} ions. Ca^{2+} is also significantly

Table 1 X-Ray data collection and refinement statistics

	Cocrystal *Bam*HI–DNA–Ca^{2+}	*Bam*HI-DNA soaked with Mn^{2+}	Cocrystal *Bam*HI–DNA–Mn^{2+} pH 7.4	Cocrystal *Bam*HI–DNA–Mn^{2+} pH 5.3
Source	CHESS	CHESS	Cu^{+2} rotating anode	Cu^{+2} rotating anode
Resolution limit(Å)	2.0	1.8	2.8	2.5
Wavelength (Å)	0.91	0.91	1.54	1.54
Unit cell	105.5, 79.4, 66.4	106.4, 79.6, 67.6	106.7, 79.6, 66.8	107.0, 79.6, 68.2
Measured reflections	93,202	11,1430	32,531	87,576
Unique reflections	31,554	40,212	11,650	19,636
R_{merge} (%)	7.4 (31.0)[1]	8.4 (31.8)	11.8 (38.8)	10.3 (33.3)
Completeness (%)	81.6 (61.0)	72.0 (45.6)	80.7 (84.9)	93.7 (97.6)
Refinement				
Reflections ($F > 2\sigma$)	29,690	33,484		
R_{factor} (%)	23.3	22.6		
R_{free}[2] (%)	25.1	26.8		
Resolution (Å)	8-2	8-1.8		
Total number of atoms	4,166	4,179		
Number of water molecules	317	352		
R.m.s. bond lengths (Å)	0.009	0.010		
R.m.s. bond angles (°)	1.5	1.7		
R.m.s. planarity (°)	1.5	1.7		
R.m.s. torsional, angle (°)	21.1	23.8		
Mean B value, overall (Å²)	21.8	30.0		
Mean B value, protein (Å²)	20.2	29.3		
Mean B value, DNA (Å²)	17.2	26.4		
Mean B value, solvent (Å²)	36.3	41.1		
B values, divalent ions (Å²)	A: 30.8, B: 24.1	A: 44.9, B: 75.8		

[1]The numbers in parentheses refer to the last resolution shells.
[2]R_{free} was calculated with 5% (Ca^{2+}) and 3% (Mn^{2+}) of data.

larger than the other cations (Co^{2+}, Zn^{2+} and Cd^{2+}) that have been shown to activate endonucleases. Finally, although the Ca^{2+} ions in our pre-reactive complex are coordinated to six ligands in an octahedral arrangement (as would be expected for Mg^{2+} or Mn^{2+}) (Fig. 2), the preference of Ca^{2+} for a higher coordination number (8) may again cause a perturbation of the transition state[31]. Overall, the inhibitory effects of Ca^{2+} on endonuclease activity appear to be rather subtle, and are probably concentrated over the transition state rather than in the initial binding to the ground state.

Together, the structures presented here provide a detailed look at both the pre- and post-reactive states of *Bam*HI. Based on the crystal structures, we propose a two-metal mechanism of cleavage for B*am*HI that is distinct from *Eco*RV. The observed diversity in metal binding in endonucleases *Bam*HI, *Eco*RV and *Eco*RI is surprising, considering the structural similarities of their active sites. However, restriction enzymes are notable for their lack of sequence similarity, which raises the question of whether they arose by convergent or divergent evolution. The diversity in metal binding may be an argument in favor of convergent evolution, though other endonuclease structures are needed for a more satisfactory answer.

Methods

Materials. The overexpression and purification protocols for *Bam*HI have been described[33]. The oligonucleotide was synthesized on a solid support using phosphoramidite chemistry. The trityl group was left on to help purify the oligomer by reverse phase HPLC, and then cleaved off with 0.1% trifluroacetic acid[34]. The purified, detritylated oligomer was eluted from the reverse phase (Dynamax 300) column with a triethylammonium acetate/acetonitrile gradient[34].

Crystallization. Cocrystals of *Bam*HI with the self-complementary 12-mer (5'-TATGGATCCATA-3'), as shown in Fig. 1*a*, were obtained by the hanging drop method at 20 °C. The protein–DNA solution contained three parts of *Bam*HI (~20–25 mg ml^{-1} in 0.5 M KCl, 20 mM potassium phosphate (pH 6.9), 1 mM dithiothreitol, 10% glycerol) to 1 part of annealed DNA (10 mg ml^{-1}). For hanging drops, 1 μl of the protein–DNA solution was mixed with 1 μl of the precipitant solution (12–14% polyethylene glycol 8000, 0.1 M MES (pH 5.3)) and set up above wells containing 12–14% polyethylene glycol 8000, 0.15 M KCl, 0.1 M MES (pH 5.3) and 5% glycerol. Birefringent crystals could be seen after a few hours as needles, which after a few days reached a size of ~0.5 × 0.1 × 0.1 mm. For the Mn^{2+} soaking experiment, a cocrystal was soaked for a total of nine hours in a solution containing the well solution at pH 5.3 plus 20 mM $MnCl_2$. Interestingly, immediately upon soaking the cocrystal showed small fractures along the shorter dimension, which healed after few minutes and the crystal remained stable afterwards. We also soaked a cocrystal with $MnCl_2$ after raising the pH of the soaking solution to 7.4 for optimal cleavage. The crystal showed greater decay at pH 7.4, but we could measure X-ray data by limiting the time of the soak to only one hour.

In addition to the soaking experiments, we attempted to cocrystallize *Bam*HI with DNA in the presence of divalent cations. (We had not attempted this in the past, based on the assumption that cleavage of the DNA would interfere with cocrystallization). Surprisingly, we obtained cocrystals in the presence of Mn^{2+} (15 mM $MnCl_2$) and Ca^{2+} (10 mM $CaCl_2$) ions under similar conditions as the native cocrystals. In all cases, the cocrystals grew best at pH 5.3 and were isomorphous to the native cocrystals (a = 108.8 Å, b = 81.9 Å, c = 68.8 Å, space group $P2_12_12_1$)[7].

Data collection. All data were collected from frozen crystals after transferring them to a stream of dry nitrogen gas (110 K). The crystals were cryoprotected by the addition of 20% glycerol to the soaking solutions. A total of four data sets were measured: Mn^{2+} soak at pH 5.3, Mn^{2+} soak at pH 7.4, Mn^{2+} cocrystals, and Ca^{2+} cocrystals. The Mn^{2+} soak at pH 5.3 and the Ca^{2+} cocrystal data were measured on beamline F1 at CHESS (λ = 0.908 Å) using imaging plates. The data from the Mn^{2+} soak at pH 7.4 and the Mn^{2+} cocrystals were collected on an R-axis II imaging plate area detector mounted on a Rigaku RU 200 rotating anode (CuKα) X-ray

generator (100 mA and 50 kV). All data were reduced to profile fitted intensities and scaled together using the HKL programs (HKL Research)[35]. To analyze the anomalous signal the Bijvoet pairs were kept separate in the scaling process. Crystal and data statistics are summarized in Table1.

Structure determination. The structures of the metal bound complexes were determined using the previously determined *Bam*HI–DNA complex[7] as a rigid-body model for rotational and translational searches as implemented in the program X-PLOR[36]. The searches were performed with data between 10 and 4 Å resolutions and resulted in initial R-factors between 32.6 and 35.8% for the different structures.

Anomalous difference Fourier maps. To determine the positions of the cations, we calculated anomalous difference Fourier maps using the FSFOUR program of the PHASES suite of programs[37]. At λ = Cu$K\alpha$, the anomalous signal (f") for Mn^{2+} is 2.8e^-, making it possible to distinguish the Mn^{2+} peaks from the random noise in the maps. At λ = 0.908 Å, corresponding to the synchrotron radiation at CHESS, the f"s for Mn^{2+} and Ca^{2+} are 1.30 and 0.57e^- respectively, making it more difficult to distinguish the metal sites from the background noise. Typically, the definition of the anomalous peaks was much improved if the maps were calculated after some cycles of refinement.

Refinement. The X-PLOR package was used to perform the refinement with the two high resolution data sets collected at CHESS, namely the Mn^{2+} soak at pH 5.3 and the Ca^{2+} cocrystal. The starting models for refinement were the rigid body solutions described above. Only data higher than 8 Å in resolution were included for refinement. The parameters for the conformational and energy terms were those derived by Engh and Huber for proteins[38], and those derived by Berman *et. al.* for DNA[39]. To assure correct DNA geometry, restraints for base planarity, sugar pucker and Watson-Crick hydrogen bonds were applied. Initially, we carried out positional refinement in which the upper resolution limit was increased each cycle (in 0.3 Å increments), to a maximum of 2.0 Å for the Ca^{2+} cocrystal and 1.8 Å for the Mn^{2+} soak. Each cycle was followed by manual rebuilding of the proteins and the DNA using the program O[40]. When the R-factor reached 30%, the individual B-factors were included for refinement after cycles of positional refinement. Once all of the electron density had been fit with the protein–DNA models, an F_o - F_c map was computed and water molecules assigned to peaks that were higher than 2σ and within hydrogen bonding distance of donor and acceptor groups on the protein and the DNA. The metal ions were included after all of the water molecules had been assigned. The positions of the metal ions in the F_o - F_c maps coincided with the peaks in the anomalous difference Fourier maps. At a later stage, when the R_{free} values were ~25%, the reflection files were modified to account for anisotropic diffraction. The final refined models contain all protein residues except some at the C-terminal arms. In the Ca^{2+} complex, the R and L arms were modeled out to residues 207 and 210 respectively. (The *Bam*HI monomer consists of 213 amino acids). In the Mn^{2+} structure, the arms R and L were traced to residues 206 and 209 respectively. In the final stages of refinement, numerous simulated annealing omit maps were computed to both check and improve the side chain positions. The refinement and model statistics are summarized in Table 1.

Coordinates. The coordinates have been deposited in the Brookhaven Protein Data Bank (accession numbers 2bam and 3bam).

Acknowledgments

We thank I. Schildkraut for stimulating discussions; R. Kucera for the purified protein; the staff at CHESS and C. Escalante, J. Hirsch, E. Jacobson, and D. Wah for help with data collection; G. Mogilnitsky and L. Shen for technical help; I. Schildkraut, L. Shapiro, and D. Wah for comments on the manuscript. This work was supported by a grant from the National Institutes of Health (A.K.A.) H.V. was supported by a Fulbright/CONACYT scholarship.

Received 18 June, 1998; accepted 27 August, 1998.

1. Roberts, R.J. & Halford, S.E. Type II Restriction Endonucleases. In *Nucleases* (eds Linn, S.M., Lloyd, R.S. & Roberts, R.J.) 35–88 (Cold Spring Harbor, New York; 1993).
2. Aggarwal, A.K. Structure and function of restriction endonucleases. *Curr. Opin. Struct. Biol.* **5**, 11–19 (1995).
3. Kim, Y., Grable, J.C., Choi, P.J., Greene, P. & Rosenberg, J.M. Refinement of *Eco*RI endonuclease crystal structure: a revised protein chain tracing. *Science* **249**, 1307–1309 (1990).
4. Winkler, F.K. *et al.* The crystal structure of *Eco*RV endonuclease and of its complexes with cognate and non-cognate DNA fragments. *EMBO J.* **12**, 1781–1795 (1993).
5. Newman, M., Strzelecka, T., Dorner, L.F., Schildkraut, I. & Aggarwal, A.K. Structure of restriction endonuclease *Bam*HI and its relationship to *Eco*RI. *Nature* **368**, 660–664 (1994).
6. Newman, M., Strzelecka, T., Dorner, L.F., Schildkraut, I. & Aggarwal, A.K. Structure of restriction endonuclease *Bam*HI phased at 1.95 Å resolution by MAD analysis. *Structure* **2**, 439–452 (1994).
7. Newman, M., Strzelecka, T., Dorner, L., Schildkraut, I. & Aggarwal, A.K. Structure of *Bam*HI endonuclease bound to DNA: partial folding and unfolding on DNA binding. *Science* **269**, 656–663 (1995).
8. Cheng, X., Balendiran, K., Schildkraut, I. & Anderson, J.E. Structure of *Pvu*II endonuclease with cognate DNA. *EMBO J.* **13**, 3927–3935 (1994).
9. Athanasiadis, A. *et al.* Crystal structure of *Pvu*II endonuclease reveals extensive homologies to *Eco*RV. *Nature Struct. Biol.* **1**, 469–475 (1994).
10. Bozic, D., Grazulis, S., Siksnys, V. & Huber, R. Crystal structure of *Citrobacter freundii* restriction endonuclease *Cfr*10I at 2.15 Å resolution. *J. Mol. Biol.* **255**, 176–186 (1996).
11. Wah, D.A., Hirsch, J.A., Dorner, L.F., Schildkraut, I. & Aggarwal, A.K. Structure of the multimodular endonuclease *Fok*I bound to DNA. *Nature* **388**, 97–100 (1997).
12. Wah, D.A., Bitinaite, J., Schildkraut, I. & Aggarwal, A.K. Structure of the restriction endonuclease *Fok*I has implications for DNA cleavage. *Proc. Natl. Acad. Sci. USA* **95**, 10564–10569 (1998).
13. Vipond, I.B., Baldwin, G.S. & Halford, S.E. Divalent metal ions at the active sites of the *Eco*RV and *Eco*RI restriction endonucleases. *Biochemistry* **34**, 697–704 (1995).
14. Pingoud, A. & Jeltsch, A. Recognition and cleavage of DNA by type-II restriction endonucleases. *Eur. J. Biochem.* **246**, 1–22 (1997).
15. Kostrewa, D. & Winkler, F.K. Mg^{2+} binding to the active site of *Eco*RV endonuclease: a crystallographic study of complexes with substrate and product DNA at 2 Å resolution. *Biochemistry* **34**, 683–696 (1995).
16. Jeltsch, A., Jurgen, A., Wolfes, H., Maass, G. & Pingoud, A. Substrate-assisted catalysis in the cleavage of DNA by the *Eco*RI and *Eco*RV restriction enzymes. *Proc. Natl. Acad. Sci. USA* **90**, 8499–8503 (1993).
17. Perona, J.J. & Martin, A.M. Conformational transitions and structural deformability of *Eco*RV endonuclease revealed by crystallographic analysis. *J. Mol. Biol.* **273**, 207–225 (1997).
18. Blundell, T. & Johnson, L.N. *Protein crystallography* (Academic Press, New York; 1976).
19. Derbyshire, V. *et al.* Genetic and crystallographic studies of the 3',5'-exonucleolytic site of DNA polymerase I. *Science* **240**, 199–201 (1988).
20. Beese, L.S. & Steitz, T.A. Structural basis for the 3'-5' exonuclease activity of *Escherichia coli* DNA polymerase I: a two metal ion mechanism. *EMBO J.* **10**, 25–33 (1991).
21. Brautigam, C.A. & Steitz, T.A. Structural principles for the inhibition of the 3'-5' exonuclease activity of *Escherichia coli* DNA polymerase I by phosphorothioates. *J. Mol. Biol.* **277**, 363–377 (1998).
22. Connolly, B.A., Eckstein, F. & Pingoud, A. The stereochemical course of the restriction enzyme *Eco*RI-catalysed reaction. *J. Biol. Chem.* **259**, 10760–10763 (1984).
23. Grasby, J.A. & Connolly, B.A. Stereochemical outcome of the hydrolysis reaction catalyzed by the *Eco*RV restriction endonuclease. *Biochemistry* **31**, 7855–7861 (1992).
24. Pan, T., Long, D.M. & Uhlenbeck, O.C. Divalent metal ions in RNA folding and catalysis. In *The RNA world* (eds. Gesteland, R.F. & Atkins, J.T.) 271–302 (Cold Spring Harbor, New York; 1993).
25. Rosenberg, J.M. Structure and function of restriction endonucleases. *Curr. Opin. Struct. Biol.* **1**, 104–113 (1991).
26. Xu, S.-Y. & Schildkraut, I. Isolation of *Bam*HI variants with reduced cleavage activities. *J. Biol. Chem.* **266**, 4425–4429 (1991).
27. Selent, U. *et al.* A site-directed mutagenesis study to identify amino acid residues involved in the catalytic function of the restriction endonuclease *Eco*RV. *Biochemistry* **31**, 4808–4815 (1992).
28. Grabowski, G., Jeltsch, A., Wolfes, H., Maass, G. & Alves, J. Site-directed mutagenesis in the catalytic center of the restriction endonuclease *Eco*RI. *Gene* **157**, 113–118 (1995).
29. Flick, K.E., Jurica, M.S., Monnat, R.J. & Stoddard, B.L. DNA binding and cleavage by the nuclear intron-encoded homing endonuclease I-Ppol. *Nature* **394**, 96–101 (1998).
30. Hensley, P., Nardone, G., Chirikjian, J.G. & Wastney, M.E. The time-resolved kinetics of superhelical DNA cleavage by *Bam*HI restriction endonuclease. *J. Biol. Chem.* **265**, 15300–15307 (1990).
31. Grosshans, C.A. & Cech, T.R. Metal ion requirements for sequence-specific endoribonuclease activity of the *Tetrahymena* ribozyme. *Biochemistry* **28**, 6888–6894 (1989).
32. Glusker, J.P. Structural aspects of metal liganding to functional groups in proteins. *Adv. Prot. Chem.* **42**, 1–76 (1991).
33. Jack, W.E. *et al.* Overexpression, purification and crystallization of *Bam*H1 endonuclease. *Nucleic Acids Res.* **19**, 1825–1829 (1991).
34. Aggarwal, A.K. Crystallization of DNA binding proteins with oligodeoxynucleotides. *Methods* **1**, 83–90 (1990).
35. Otwinowski, Z. & Minor, W. Processing of X-ray diffraction data collected in oscillation mode. *Meth. Enz.* **276** 307–326 (1997).
36. Brunger, A.T. *X-PLOR (version 3.0) Manual.* (Yale University, New Haven, Connecticut; 1992).
37. Furey, W. & Swaminathan, S. PHASES-95: A program package for the processing and analysis of diffraction data from macromolecules. *Meth. Enz.* **277**, 590–620 (1997).
38. Engh, R.A. & Huber, R. Accurate bond and angle parameters for X-ray protein structure refinement. *Acta Crystallogr. A* **47**, 392–400 (1991).
39. Parkinson, G., Vojtechovsky, J., Clowney, L., Brunger, A.T. & Berman, H.M. New parameters for the refinement of nucleic acid containing structures. *Acta Crystallgor. D* **52**, 57–64 (1996).
40. Jones, A.T., Zou, J.Y., Cowan, S.W. & Kjeldgaard, M. Improved methods for building protein models in electron density maps and the location of errors in these models. *Acta Crystallogr. A* **47**, 110–119 (1991).